Synthesis and Characterization of MNPs Hydrogel with pH-Responsiveness Properties to Release Diclofenac Sodium as a Model Drug

Ghobadifar, Vahid; Bagheri Marandi, Gholam*[+]; Kurdtabar, Mehran
Department of Chemistry, Karaj Branch, Islamic Azad University, Karaj, I.R. IRAN

Rezanejad Bardajee, Ghasem
Department of Chemistry, Payame Noor University, Tehran, I.R. IRAN

***ABSTRACT*:** *In the present study, the loading and releasing of Diclofenac Sodium (DS) were investigated using a pH-sensitive magnetic nanocomposite hydrogel. The hydrogel was prepared through grafting copolymerization of Acrylic Acid (AA) and acrylamide (AAm) and using ammonium persulfate (APS) as a free radical initiator in the presence of Fe_3O_4@SiO_2@(3-Aminopropyl) trimethoxysilane (APTMS)@Maleic anhydride (MAN) as a cross-linker. The nanocomposite hydrogel structure (Fe_3O_4@SiO_2@APTMS@MAN) was confirmed as the result of XRD, VSM, FT-IR, SEM, EDS, and TEM spectroscopy techniques. Furthermore, thermal properties were deliberated using TGA and DTG. The effects of different parameters such as pH, time, Fe_3O_4@SiO_2@APTMS@MAN content, and salt solutions on swelling behavior were investigated considering the abovementioned outcomes. The adsorption isotherm was studied at 25°C using Langmuir, Freundlich, and Temkin. The adsorption data were well described by the Langmuir isotherm model. A kinetic study revealed the applicability of pseudo-first-order and pseudo-second-order models for the adsorption of mentioned DS. Moreover, the pH sensitivity of nanocomposite hydrogel and loading/releasing drugs were studied. Examining in vitro drug release in different buffer solutions indicated that the pH of the solution could mainly lead to the DS drug-releasing behavior of hydrogel. However, the cumulative release ratio of DS in pH: 7.4 solutions reached up to 93% within 120 min. Consequently, the investigated nanocomposite hydrogel of this study (Fe_3O_4@SiO_2@APTMS@MAN) can be applied in widespread biomedical applications, particularly for controlled, targeted drug delivery purposes.*

KEYWORDS: *Controlled drug release; Diclofenac sodium; Hydrogels; Magnetic nanocomposite; pH sensitivity.*

INTRODUCTION

Hydrogels are hydrophilic 3D polymeric networks that could be swollen in aqueous or biological media despite water-insolubility due to their matrix structure [1]. Hydrogels have been extensively used in various fields of applications, including drug delivery [2], color absorption [3], biochemical applications [4], catalysis [5], and water

***** *To whom correspondence should be addressed.*
+ *E-mail: marandi@kiau.ac.ir*
1021-9986/2023/3/875-889 *15/$/6.05*

treatment [6]. Nevertheless, weak mechanical stability and partial stimuli-responsive ability might restrict the usage of hydrogels for specified functions [7]. To solve such a problem, iron, nickel, manganese, or cobalt-based nanoparticles were embedded in the 3D hydrogel networks to improve the desired functions [8]. In this case, those iron-based nanoparticles have been heeded due to their remarkable features of particle sizes, high degrees of biocompatibility, and safety for medical applications [9]. The nanoparticle can be coated by a layer of functional silica to develop stability and provide a surface for attaching further functional groups for hydrophilic improvements [10]. Indeed, magnetic nanoparticles (MNPs) have been used as the chemical cross-linker of the hydrogel network to improve mechanical properties, swelling capacity, and drug loading/releasing ability [11]. In order to provide the pH-sensitive hydrogels, vinyl monomers with different acidic and basic functional groups such as acrylic acid (AA) and acrylamide (AAm) have been used for hydrogel synthesis. Excellent water lock ability and water imbibition rate of these three-dimensional cross-linked polymers can range from a hundred to several thousand times their weight [12].

Chen J. et al. have noticed the use of magnetic hydrogels for different purposes in recent years, in which methylene blue and neutral red are absorbed by PAsp-PAA/Fe_3O_4 hydrogel [13]. Strain-stiffening and self-healing hydrogels have been synthesized to provide artificial tissue scaffolds and wound dressings [14]. Nanocomposite hydrogels have been used as photon-like catalysts to degrade antibiotic contaminants and drug release usages, e.g., magnetic nanocomposite of Fe_3O_4/SiO_2/HAP has already been used for atenolol delivery in addition to examining toxicity in vivo [15,16]. Various protocols have been proposed to employ nanoparticles for such critical targeted drug delivery processes [17]. For example, the controlled releasing process of doxorubicin under an alternating magnetic field has been investigated using a magnetic molecularly imprinted polymer nanoparticle in thermal conditions [18]. Therefore, it is essential to carry out more studies in this field to develop more protocols for specified uses.

In the present study, a magnetic nanocomposite hydrogel was provided by copolymerization of AA and AAm counterparts in the presence of Fe_3O_4@SiO_2@APTMS@MAN nanoparticle (MNPs). The loading/releasing of diclofenac sodium (DS) was examined for the nanocomposite hydrogel at pH 7.4 for controlled drug delivery processes. Furthermore, the effects of nanoparticle magnitudes on hydrogel swelling and pH sensitivity for the attached DS were carefully examined. Consequently, essential information was provided to discuss the main problem of this work on examining the advantage of using such MNP_S hydrogel for DS-targeted drug delivery purposes.

EXPERIMENTAL SECTION

Materials

Hydrochloric acid (HCl, Merck 25%), ferrous chloride tetrahydrate ($FeCl_2 \cdot 4H_2O$, Merck 99%), and ferric chloride anhydrous ($FeCl_3$, Merck 98%) reagents were utilized for Fe_3O_4 magnetic nanoparticle preparation. Tetraethyl orthosilicate (TEOS), (3-Aminopropyl) trimethoxysilane (APTMS, Merck), Maleic anhydride (MAN, Merck), N, N-dimethylformamide (DMF, Merck) and (Pyridine, Merck) were employed for silica coating modification of nanoparticles. Acrylic acid (AA, Merck) and acrylamide (AAm, Merck) monomers, and ammonium persulfate (APS, Sigma-Aldrich) initiator were used to synthesize the polymer backbone of the hydrogel. Diclofenac sodium (DS) (Fig. 1) was obtained from Tavan Research and Educational Institute (Tehran, Iran) for loading at the nanocomposite hydrogel and examining in vitro release.

Instruments

The surface morphology of hydrogel was observed through a field-emission scanning electron microscope (FESEM; SIGMA VP, ZEISS, Germany) equipped with an energy-dispersive X-ray analysis system (EDS; Oxford Instrument, UK). The particle size was measured by transmission electron microscopy (TEM; ZEISS-em10c-100kv-Germany). FT-IR spectra were recorded between 400 and 4000 cm^{-1} (Thermo, AVATAR FT-IR spectrometer, USA). X-ray diffraction pattern of the nanocomposite hydrogel was recorded on a low-angle X-ray diffractometer (XRD; PHILIPS, PW1730, step size = 0.05 deg, time step = 1 s, 40 kV, 30 mA, Netherlands). The magnetic properties of the product were measured on a vibrating sample magnetometer (VSM; LBKFB, Magnates Daghigh Kavir Company, Iran). ThermoGravimetric Analysis (TGA; Q600, TA, USA) and ultraviolet-visible

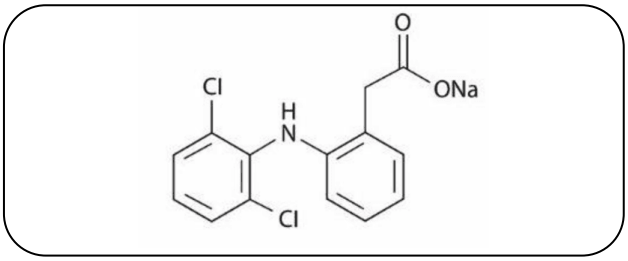

Fig. 1: Chemical structure of diclofenac sodium.

absorption spectra (UV-VIS, Shimadzu UV-Vis 2401, Japan) were also recorded.

Preparation of magnetic nanoparticles (Fe_3O_4)

The MNP was prepared by the conventional coprecipitation method. Initially, 30 mmol of anhydrous $FeCl_3$ and 10mmol of $FeCl_2.4H_2O$ were dissolved in 50 mL of 0.5 M HCl solution. Subsequently, the solution containing iron ions in a 3:1 M ratio of Fe (III): Fe (II) was added dropwise to 500 mL of 1.5 M sodium hydroxide solution at 80 ℃ under a 40 mL/min nitrogen flow with strenuous stirring. The MNP was precipitated with a magnet, thoroughly washed with deionized water, and finally dried at 50 ℃ under vacuum conditions for four hours [19].

Preparation of silica coating of magnetic nanoparticle (Fe_3O_4@SiO_2)

A sample of 2 g of prepared Fe_3O_4 MNP was completely dispersed in a solvent mixture of ethanol (320 mL) and deionized water (80 mL) for 30 min at room temperature. First, the pH of the solution was adjusted to 10 using ammonia solution, then 8 mL of TEOS in 10 mL of ethanol was gradually added. After mechanical agitation at room temperature for 24 h, the collected product was washed with ethanol and deionized water three times, and it was eventually dried under vacuum conditions at 50 ℃ [20].

Surface modification

a) Fe_3O_4@SiO_2

Surface modification of Fe_3O_4@SiO_2 was done by APTEMS, yielding plentiful double bonds at the surface. A sample of 2 g of Fe_3O_4@SiO_2 was dispersed in a mixture of ethanol (100 mL) and deionized water (25 mL), and 16 mL of APTEMS was gradually added to the reaction mixture after solicitation and stirred for 10 min in a three-neck flask. The reaction mixture was stirred for 24 h at 60 °C. The final magnetic product was washed several times using ethanol and deionized water to remove excess APTEMS, and it was collected with the contribution of a magnet to be dried in a vacuum oven at 50 ℃ overnight.

b) Fe_3O_4@SiO_2@APTMS@MAN

First, a sample of 2 g of Fe_3O_4@SiO_2@APTMS was dispersed in 105 mL of DMF under nitrogen gas. Next, 2.674 g of MAN and 1.19 mL of pyridine were added to the dispersion. The final mixture was stirred at 50 ℃ for 3 h. During the reaction, the color of the mixture was changed from colorless to bronze. The product was washed using toluene and ethanol three times and dried at 60 °C overnight to achieve Fe_3O_4@SiO_2@APTMS@MAN [21].

Preparation of Fe_3O_4@SiO_2@APTMS@MAN hydrogel

The polymerization reaction was carried out in a 250 mL three-neck flask equipped with ultrasound waves to provide the Fe_3O_4@SiO_2@APTMS@MAN hydrogel. Primarily, different nanoparticles, including MNP_SH1, MNP_SH2, and MNP_SH3 with (0.6, 0.75, and 0.9 g), respectively, and 25 mL of deionized water were sonicated (160 W) for 20 min before the synthesis procedure. Next, 1 mL of acrylic acid and 3 mL of acrylamide (each dissolved in 5 mL of deionized water) were added to the reactor. Afterward, 0.2 g of APS dissolved in 5 mL of deionized water was added to the reactor up to completing the reaction after 150 min under heat treatment. Subsequently, the reactor was taken out of the bath and cooled down to room temperature. The produced MNP_SH was separated into smaller pieces. An amount of 0.41g NaOH (the equivalent of 10.2 mmol/lit) was dissolved in 10 mL of water and poured into the reactor under agitation for 5 min neutralize 70 % of carboxylic acid groups (functional groups of AA) from the reaction environment. MNP_SH was left for one hour to allow the neutralization process to be completed. Then, the product was transferred into a 250 mL ethanol solution to eliminate water and other contaminations (like non-reacted monomers and soluble polymers). After about three hours, the MNP_SH was dewatered, removed from ethanol, and put in the oven at 50 ℃ for two days to be dried completely [19].

Swelling measurement

a) Swelling in distilled water

Gravimetric analysis was used to reflect the swelling ratio of synthesized MNP_SH1, MNP_SH2, and MNP_SH3. Primarily, 0.05 g of the dried hydrogel powder was put

into a tea bag (i.e., a 100-mesh nylon screen). For the next step, it was placed in a beaker containing 200 mL of deionized water to attain equilibrium at room temperature for 120 min. The swollen detached hydrogels from the swelling media were measured at further gaps before removing surplus water. The polymer hydrogel's swelling ratio (*SR*) was determined using Eq (1).

$$SR = \frac{W_2 - W_1}{W_1} \quad (1)$$

Where W_1 and W_2 are the weights of dried and swollen samples, respectively.

b) Swelling in various salt solutions

Parallel experiments and calculations were performed to detect salt effects on the swelling behavior of MNP_SH. Immersing a known amount of MNP_SH1, MNP_SH2, and MNP_SH3 in a salt solution of NaCl, KCl, $CaCl_2$, $MgCl_2$, and $AlCl_3$ with Specific concentration at room temperature led to display effects of different types of salt solutions on the swelling behavior of MNP_SH [22].

pH sensitivity

A sample of 0.05 g of the MNP_SH1, MNP_SH2, and MNP_SH3 was plunged in a 200 ml buffer solution with a pH range between 1 to 12 values at equilibrium for 120 min to reach swelling divided from unabsorbed water. The media was then filtered using a 100-mesh screen under gravity for 30 min without blotting the sample. The swelling ratio in buffer solution was calculated according to Eq. (1). Buffer solutions with various pH were prepared to exploit acidic and basic buffer solutions like hydrochloric acid, potassium chloride, sodium citrate dihydrate, citric acid, sodium phosphate dibasic heptahydrate, sodium phosphate monobasic monohydrate, ammonia and ammonium chloride. They were adjusted to 0.2 M with NaOH and HCl solutions settled with a pH meter [23].

Drug absorption

Aqueous solutions of DS with initial concentrations of 50, 75, 100, and 125 mg/L at pH 7.4 were stirred to realize the effect of dosage on the absorption capacity of DS. To this point, 0.05 g of MNP_SH was added and swelled at room temperature for 8 h. A polytetrafluoroethylene (PTFE) 0.22 μm syringe filter was used to separate the DS solution from swollen MNP_SH. DS concentration was determined by dint of a spectrophotometer at 276 nm, and the amount of DS was computed using Eq (2).

$$q_e = \frac{(c_0 - c_e)V}{M} \quad (2)$$

Where C_0 and C_e represent the initial and equilibrium concentrations of DS, respectively, *V (L)* is the volume of the solution, and *M (g)* is the mass of the used MNP_SH [24].

In vitro releasing

DS drug-releasing from MNP_SH was analyzed at 37 °C in PBS solution in vitro. 0.05 g of MNP_SH was added to 20 ml of the aqueous solution, to which 100 mg of DS was already dissolved. The drug-containing MNP_SH was placed in a freeze dryer to get dried. Next, 100 mL of Phosphate-Buffered Saline (PBS) buffer solution was added to the dried sample to release DS gradually. At given time intervals, 1 mL of release medium was removed using a PTFE 0.22 μm syringe filter, and, after suitable dilution, UV spectrum at 276 nm was used to measure released DS concentration, and drug release percent was calculated using Eq (3).

$$\text{Released drug (\%)} = \frac{R_t}{L} \times 100 \quad (3)$$

Where L and R_t represent the initial amount of drug loaded and the final amount of drug released at time t, respectively [25].

RESULTS AND DISCUSSION

Synthesis of MNPsH

The MNP_SH was synthesized by graft copolymerization of AA and AAm copolymerization through free-radical copolymerization in the presence of MNP_S as a cross-linker (Scheme 1). Copolymerization is based on the hypothesis of forming free radical sites on nanoparticles and monomers, i.e., AA, AAm, by decomposition of persulfate at 85 °C as initiator and then polymerization of monomers from these radical sites. At the same time, MNPs were also applied to induce magnetic features in the hydrogel. During polymerization, MNPs are diffused and dispersed in the polymer matrix. Due to the dual bonding of the monomers and MNPs as cross-linker, the anionic sulfate radicals begin the polymerization process and form a 3D network of MNP_SH.

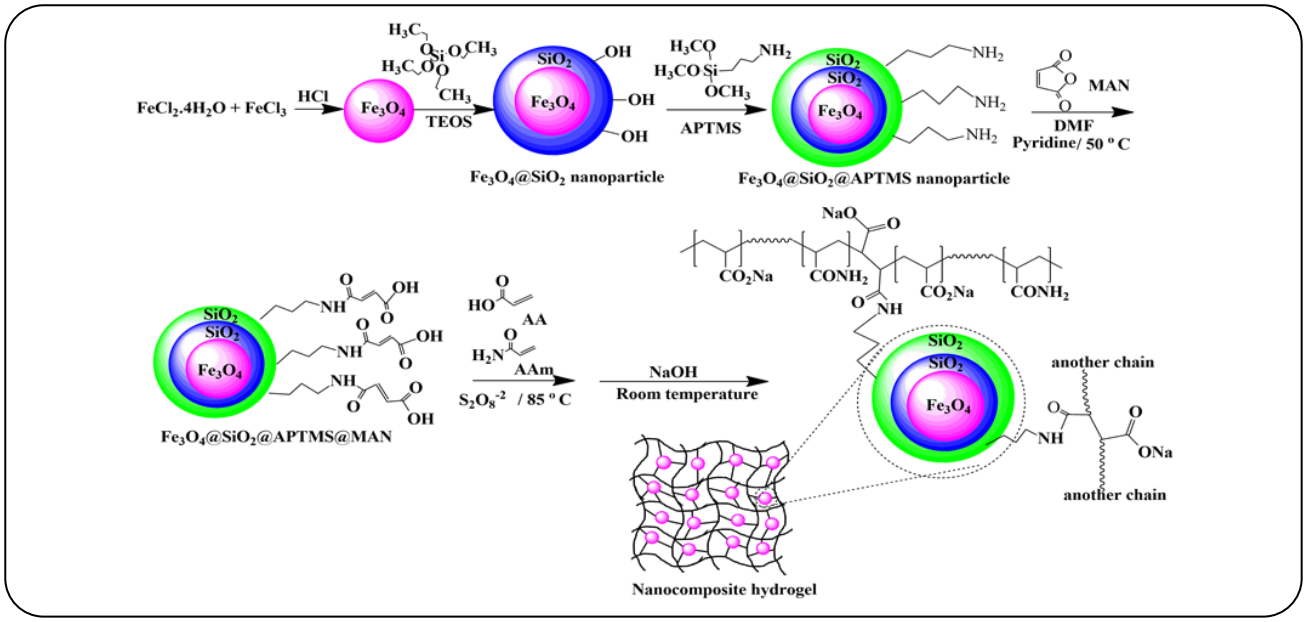

Scheme 1: The proposed mechanism for preparation of MNPsH.

FT-IR spectroscopy

The recorded *FT-IR* spectra of MNP_S, MNP_SH3, and DS-loaded MNP_S H3 are illustrated in Fig. 2. The absorption band at 570 cm^{-1} was attributed to Fe-O-Fe vibration, and the Si-O-Si vibrations reached a sharp peak at 1099 cm^{-1}. Furthermore, the peaks at 1631 cm^{-1} and 3437 cm^{-1} were assigned to the absorbed water and hydroxy groups, respectively, related to MNP_S. Also, in MNP_SH3, they showed a broad peak at 2500–3500 cm^{-1}, corresponding to the O–H stretching vibrations of carboxyl, Si-OH, and –NH units in used monomers. The characteristic vibration peak at 1651 cm^{-1} was attributed to the stretching vibrations of the C=O bond in the carbonyl groups. Bands at 1448 cm^{-1} were attributed to the C–H bending vibration. Eventually, the peaks around 1281 and 1159 cm^{-1} were attributed to the stretching vibrations of C-O (carboxyl) and C–N (amide) functional groups in the polymer chain, respectively. Nevertheless, the sharp peaks of -NH and –C=O groups arose at 1690 cm^{-1} and 1452 cm^{-1} for DS, respectively, related to DS-loaded MNP_S H3. These data confirmed the successful synthesis of MNP_SH [26]

Scanning electron microscopy (SEM)

Hydrogel microstructure morphologies are among the essential features to be carefully inspected for characterization purposes. The surface morphology of the samples was examined by scanning electron microscopy (SEM). Panels a-c of Fig. 3 presented

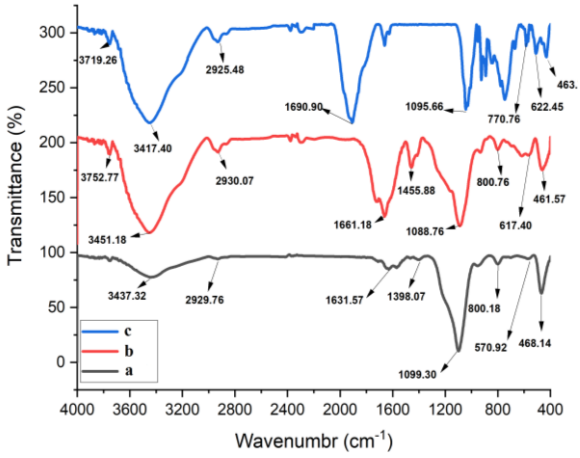

Fig. 2: FT-IR spectra of a) MNPs, b) MNPsH3 and c) DS loaded MNPsH3.

the recorded SEM images of MNP_S, MNP_SH3, and DS-loaded MNP_SH3 taken at low and high magnification.

The nanoparticles with a spherical or quasi-spheroidal shape were observed with a quite uniform size distribution (a1-a3). The panels (b1-b3) revealed cross-linking interconnected MNP_S. Also, it is obvious that the outer surface of the MNP_S is more homogeneous, continuous with agglomeration in comparison with MNP_SH. The incorporation of MNP_S with monomers led to rough outer morphology. The panels (c1-c3) the pores built on the surface

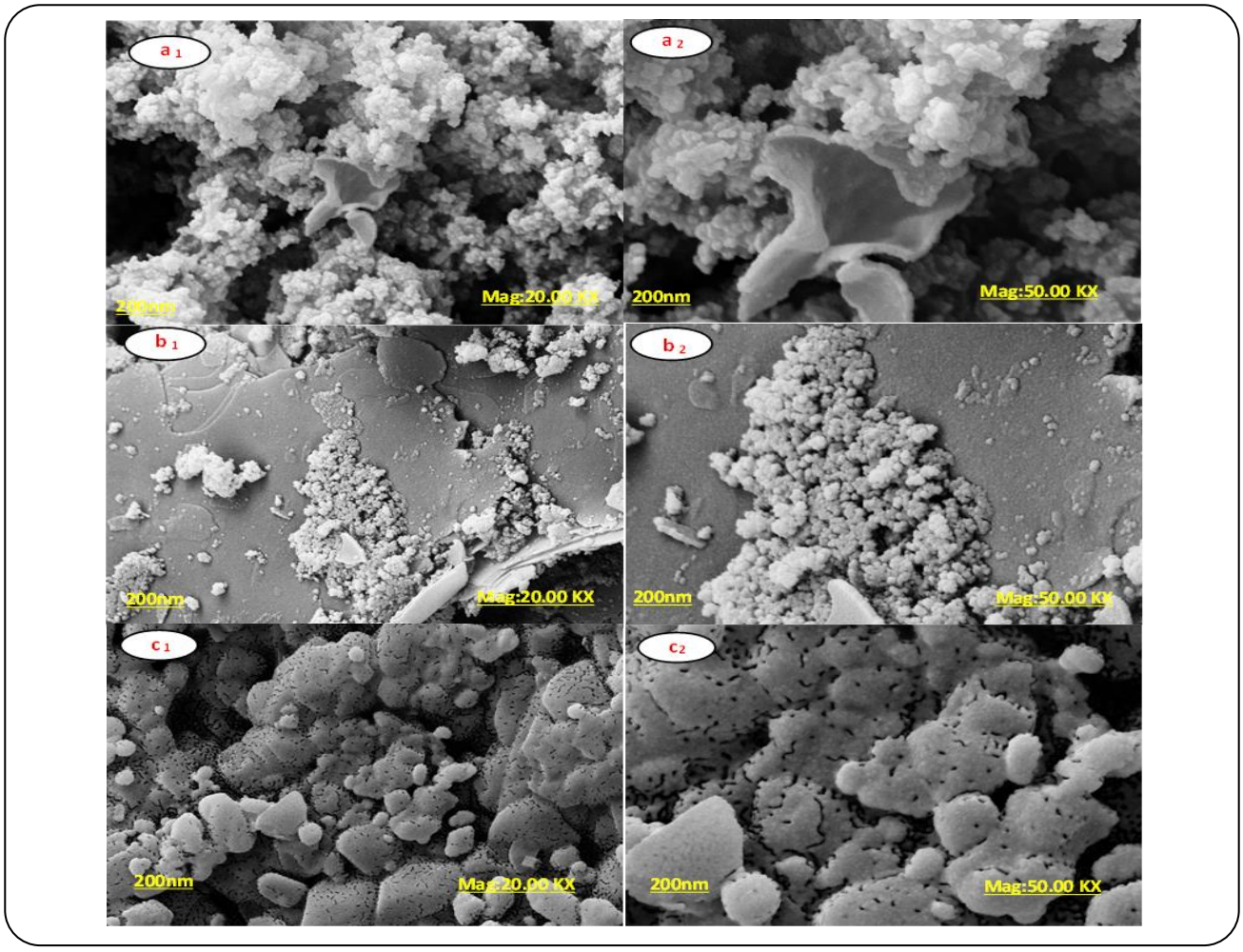

Fig. 3: SEM spectra of a) MNPs, b) MNPsH3 and c) DS loaded MNPsH3.

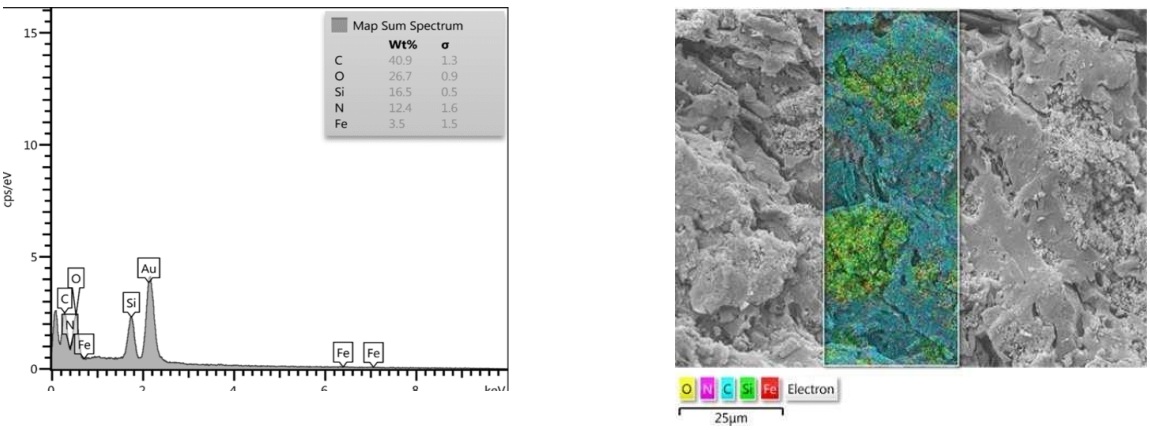

Fig. 4: EDS spectra of MNPsH3.

of the MNP_SH3 indicated DS particles loaded on the porous surface and pores of an MNP_SH3. Moreover, Fe and Si peaks in the EDS spectrum of nanoparticles in the MNP_SH3 were evidenced in Fig. 4 [27].

Transmission Electron Microscopy (TEM)

The recorded TEM images for both MNP_S and MNP_SH3 were revealed at low and high magnification in the a and b panels of Fig. 5. Spherical morphology and

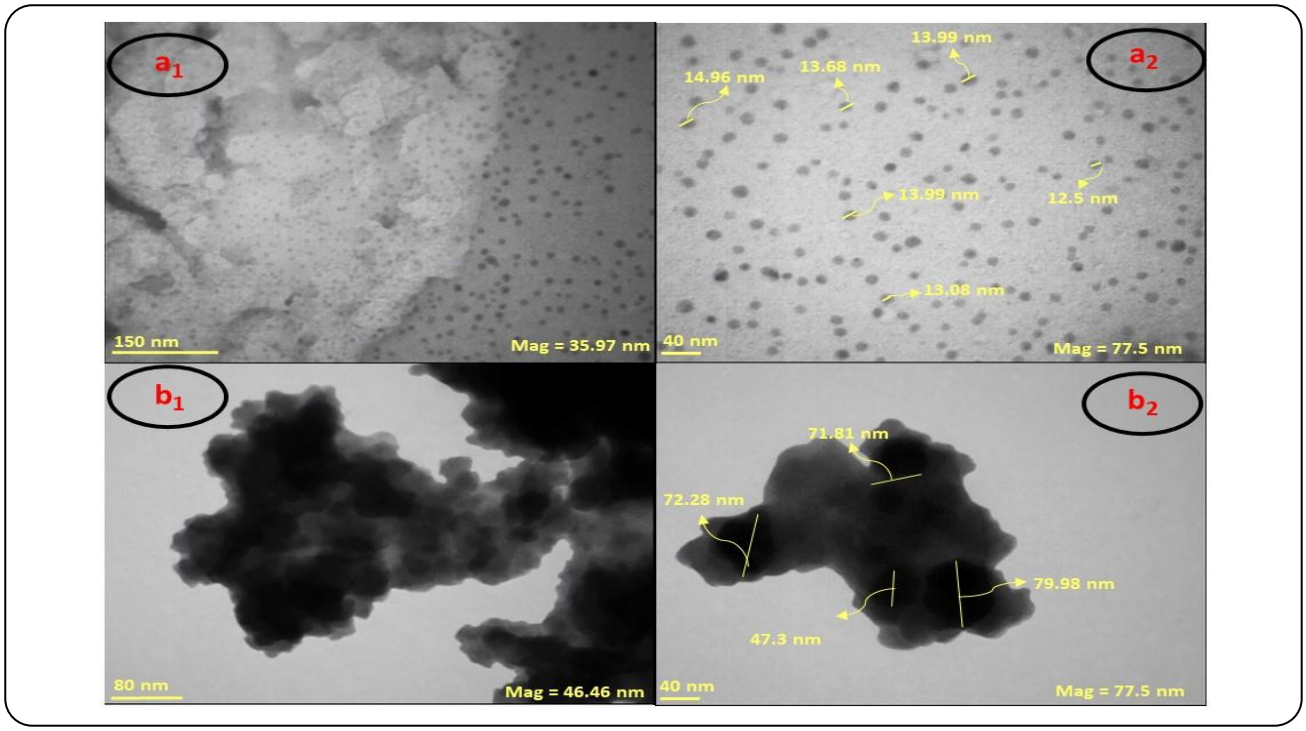

Fig. 5: TEM spectra of a) MNPs and b) MNPsH3.

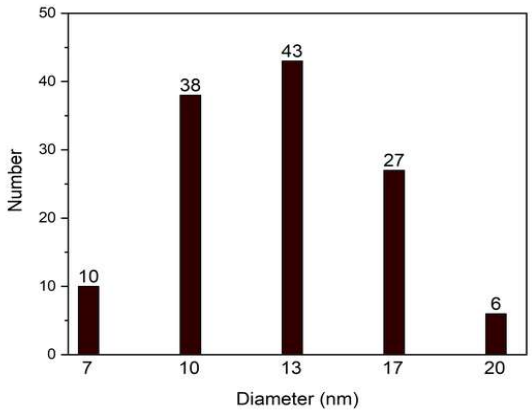

Fig. 6: Distribution of particles size of TEM image (a2).

uniform dispersion were proved by analyzing TEM images (a1-a2). Besides, the images presented the core-shell structure of nanospheres with a dark core and bright layer. Likewise, the formed thick layer proved that the nanoparticles were employed as a cross-linker in the polymerization of MNP_SH3, as shown in panels b1-b2.due to the Fig. 6, related to TEM image (a2), this image has shown distribution of particle size and the average particle size that be 13 nm. However, particle size of the MNP_S and uniform distribution on the polymer matrix, the MNP_SH was successfully made.

Vibrating-sample magnetometer (VSM)

Fig. 7 shows the usual magnetization curves of MNP_S and MNP_SH3. As is evident, the saturated magnetic field (Ms) of MNPs and MNP_SH3 were 0.75 and 0.20 emu/g, respectively. Next, the saturation of MNP_S was much more than that of MNP_SH3, due to coating of magnetic core with SiO_2 and APTMS layers the magnetic saturation (Ms) value of the nanocomposites significantly decreases. Also, the formation of covalent bonds of monomers with the magnetic nanoparticles decreases the surface spin disorder of the nanoparticles which expedited the decreases of the Ms value of the nanoparticles. VSM diagrams revealed that the MS of the produced sample is enough for separation by the external magnetic field [28].

X-ray deification (XRD)

The recorded XRD spectra of MNP_SH3 and MNP_S are shown in Fig. 8. The characteristic peaks of Fe_3O_4 as core about (2θ = 28, 37, 41, 48, and 59) showed that the crystalline structure of Fe_3O_4 nanoparticles is a face-centered cubic structure. Also, the peak in 2θ = 22 could be allocated to the existence of SiO_2 amorphous structure, which proved the stability of crystalline structure by the modified nanoparticle. These diffraction peaks were observed in MNP_SH3 and confirmed the presence of MNP_S in the MNP_SH3 structure [29].

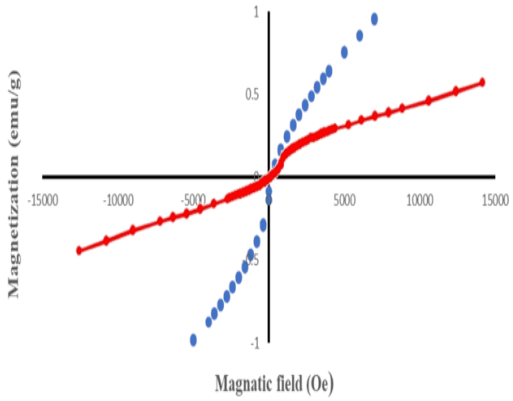

Fig. 7: VSM spectra of the MNPs (blue) and MNPsH3 (red).

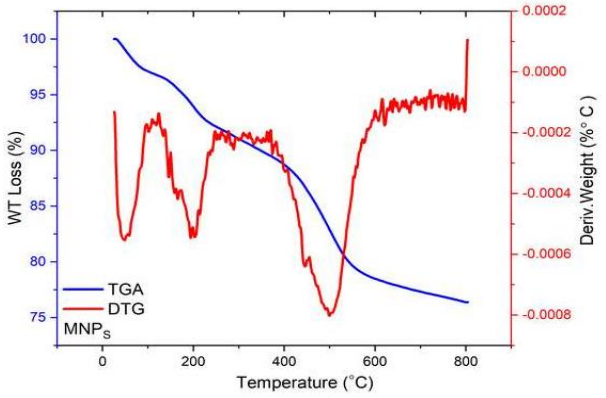

Fig. 9: Thermal analysis of the MNPs.

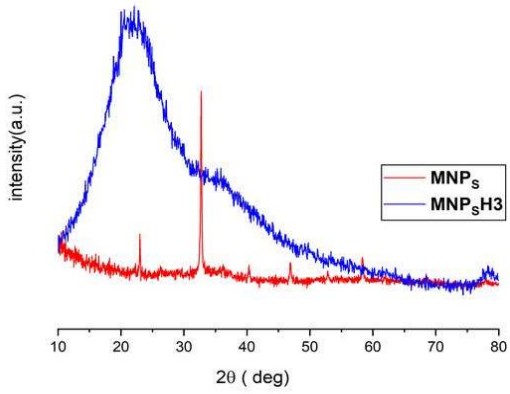

Fig. 8: XRD spectra of the MNPs (red) and MNPsH3 (blue).

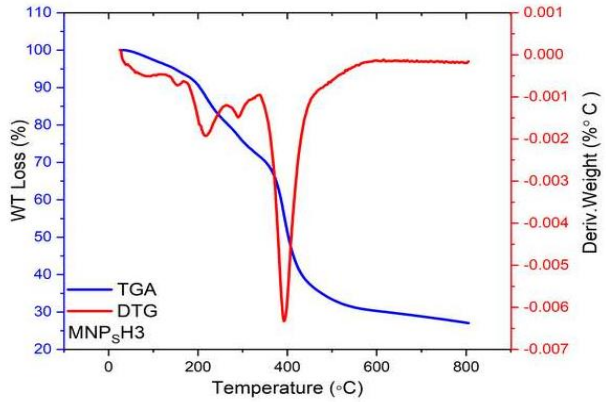

Fig. 10: Thermal analysis of the MNPsH3.

Thermo gravimetric analysis (TGA)

Figs. 9 and 10 clarified the recorded ThermoGravimetric Analysis (TGA) and Derivative Thermogravimetric (DTG) curves of MNP_S and MNP_SH3 calculated in the range of 0 to 800 °C. The weight losses of MNP_S and MNP_SH3 occurred below 100 °C because of the omission of absorbed water molecules and volatile organic components. Increasing temperature from 325 to 425 °C subjected to a significant weight loss of MNP_S due to the failure of C-O bonds and even water of anhydrides during the reaction. In the temperature range of 500 to 800 °C, the weight of the sample sharply declined. Because of the C-C thorough bond destruction at 850 °C, 20% of the weight remained. As the results of DTG, there were three apexes in the MNP_S thermogram, which were endothermic. The first peak was placed from 125 to 225 °C, presenting the loss of volatile compounds and water. The second peak was placed at 325 to 425 °C s due to the decomposition of linked APTMS molecules. Based on the recorded thermogram of MNP_S with soaring temperature in the range of 425 to 625 °C, the endothermic peak occurred at around 600 °C owing s ascribed to the phase transition from magnetite (Fe_3O_4) to hematite (Fe-O) structure. As a result, the Fe-O is thermodynamically stable above 525 °C in the phase diagram of the Fe-O system, followed by decreasing due to deoxidation of Fe-O. Moreover, there were two apexes in the MNP_SH3 thermogram. The First peak was located at 140 to 225 °C providing the broken MNP_SH3 polymer at 200 °C. At temperatures from 425 to 525 °C, the second peak was located at the oxidation of MNP_SH3 at 510 °C. The TGA and DTG results indicated that the MNP_SH was successfully synthesized [30].

Swelling

a) Swelling in distilled water

Swelling behavior in the drug delivery system is important to understand depending on the amount of water absorption by hydrogel, in which more water

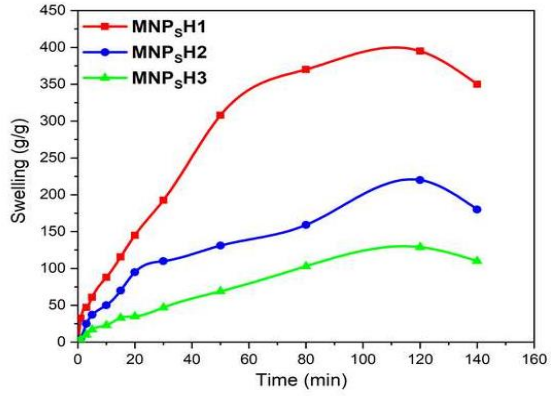

Fig. 11: Swelling of MNPsH in distilled water. Conditions: absorbent dose, 0.05g/L and temperature 25 °C.

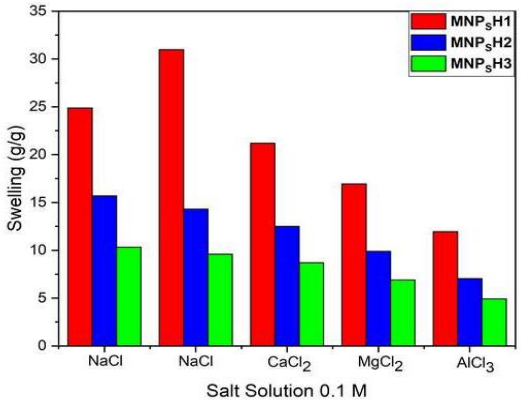

Fig. 12: Swelling of MNPsH in different salt solution. Conditions: C0, 0.1M; absorbent dose, 0.05g/L and temperature 25 °C.

absorption could lead to more drug diffusion. Several factors, such as cross-linking density of hydrogel network, hydrophilicity and hydrophobicity of polymers, and pH of hydrogels, could display dominant impacts on swelling behavior. Swelling index in distilled water as a function of time presented that the first swelling increased quickly after immersing in water, reaching equilibrium within 120 min, then slowly decreased. Maximum swelling of 395 g/g after 120 min was observed by MNP_SH1. Enhancing the number of MNP_S in the MNP_SH could decrease the amount of water swelling because of the contraction of the hole created on the surface of the MNP_SH. Fig. 11 specifies the swelling of MNP_SH in distilled water [31].

b) Swelling in various salt solutions

Numerous studies indicated the significant effects of the properties of external solutions on the rate of swelling of hydrogels. Such properties could be categorized as the type of soluble salts, the concentration of soluble salts, the number of charges, the ionic strength, and the properties of hydrogels, such as nature. Network elasticity, the existence of hydrophilic functional groups in the structure of the polymer, and the density of the lattice are those essential properties of polymers.

The swelling rate of the synthesized anionic hydrogels in different saline solutions is drastically reduced compared to the maximum measured amount in distilled water. The main reason for such variation is attributed to the overlap of the cations causing the anion-anion electrostatic repulsion to be superior. In this case, the osmotic pressure difference is reduced due to the concentration difference of the moving ion between the gel phase and the aqueous phase. Also, the effect of polyvalent ion networking is another reason for the decrease in swelling in hydrogels due to increased cross-links in the hydrogel. Therefore, with increasing the capacity and concentration of ions in solution, a decrease in adsorption should be observed, as shown in Fig. 12.

Swelling in buffer solutions

Specimens were placed in different buffer solutions at room temperature to reach equilibrium time and assess pH's influence on swelling features of MNP_SH samples. The pH of the solution varied from 1 to 12, and the swelling response was checked against each pH solution Fig. 13 revealed the swelling ratios. According to the observations, the swelling particularly influenced neutral pH against the acidic and basic conditions. MNP_SH1 presented the maximum swelling against the other samples. The amount of hydrogel inflation increases by increasing the pH value from 1 to 7 while reducing in the pH range from 8 to 12. PKa Polyacrylic acid is about 4.5; when pH is less than pKa, H^+ ionic strength is high, which effectively influences the ionization of carboxylic acid groups. Thus, the gel is neutral in acidic pH, and the flexibility of polymer chains is relatively low. When the pH of the environmental solution is higher than pKa, carboxylic acid groups in the polymer network-wide are ionized in the form of COO^-, and they attract H^+ in the gel area. Therefore, with the fully effective increase of free ions concentration inside the nanocomposites, due to increasing ionic inflation pressure, nanocomposites have a greater tendency to spread, and thus the maximum

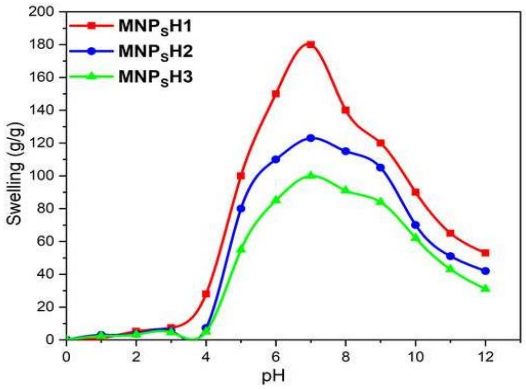

Fig. 13: Effects of pH of solution on swelling MNPsH. Conditions: absorbent dose, 0.05g/L, pH 1 to 12 and temperature 25 °C.

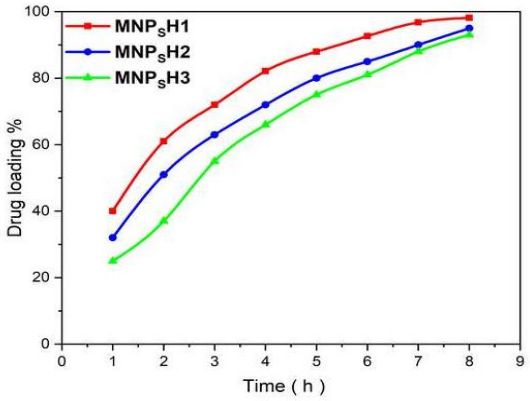

Fig. 14: Effects of MNPs (cross linker) content on DS loading Conditions: Concentration of DS, 100 mg/L and temperature 25 °C.

repulsion will occur between ionized carboxylate groups. The maximum absorption of nanocomposite hydrogel is at PH: 7. At higher pHs, Na^+ cations were derived from NaOH cover COO^- groups and prevented the effective cation-anion repulsion [32].

Drug loading efficiency

The drug loading of MNP_SH with different cross-linker contents is shown in Fig. 14. As observed, the amount of drug-loaded in the MNP_SH beads decreased as the MNP_S (cross-linker) content increased. The increase in crosslink density decreased the swelling of the hydrogel, and, accordingly, the amount of drug-loaded into the hydrogel decreased [33].

Absorption equilibrium study

Equilibrium isotherm studies were used to consider experimental sorption data employing several models such as Langmuir, Freundlich and Temkin to explain adsorption equilibria.

a) The Langmuir isotherm

The Langmuir model is probably the best known and most broadly utilized sorption isotherm. The Langmuir isotherm is based on monolayer adsorption on the solid surface with identical and homogeneous sites, as described in Eq (4).

$$q_e = \frac{q_{max}\, b\, Ce}{1 + b\, Ce} \qquad (4)$$

Where q_e is the quantity of adsorbed DS at equilibrium (mg/g), q_{max} is the maximum adsorption capacity of adsorbent (mg/g) and b (L/mg) is the adsorption equilibrium constant. In this adsorption isotherm model, the adsorption layer is anticipated to coat only one molecular layer with no interaction between them on adjacent sites, and all the adsorption sites have uniform energy. The eventuality of the adsorption process is computed by the value of the separation factor (*RL*, known as the equilibrium parameter), which is obtained using Eq (5).

$$R_L = \frac{1}{1 + bC_0} \qquad (5)$$

Where C_0 is the initial DS concentration (mg/L) and b is the Langmuir constant. Using the value of R_L, the effect of the isotherm process has been evaluated to anticipate whether an adsorption system is desirable or undesirable. The isotherm will be undesirable, linear, desirable, and invariable for $R_L > 1$, linear for $R_L = 1$, favorable for ($0<R_L<1$) and invariant for $RL = 0$.

b) The Freundlich isotherm

The Freundlich isotherm is an empirical model based on multilayer sorption between equilibrium solid and liquid phases. Freundlich assumes the adsorption areas are distributed exponentially concerning the heat of adsorption. The Freundlich equation can be described by Eq (6).

$$q_e = k_F\, c_e^{1/n} \qquad (6)$$

Where *1/n* and K_F are the intensity of adsorption and multilayer adsorption capacity, respectively, the adsorption is favorable when the *1/n* value is between 0 and 1.

c) The Temkin isotherm

The adsorption characteristic can be defined according to the Temkin model based on the assumption that the adsorption is characterized by a uniform distribution of binding energies and the heat of adsorption of all molecules in the layer decreases with coverage due to adsorbent-adsorbate interactions. This model is expressed using Eq (7).

$$q_e = \frac{RT}{\beta} \ln K_t C_e \quad (7)$$

Where β *(=RT/b)* is a constant relevant to the heat of adsorption (kJ/mol), and K_t is the equilibrium binding constant (L/g) relevant to the maximum binding energy.

The isotherm parameters of Langmuir, Freundlich, and Temkin models are presented in Table 1. Accordingly, the correlation coefficient (R^2) of the Langmuir model is higher than that of the other isotherm models approaching unity. Thus, the Langmuir isotherm is more appropriate to describe the experimental data. The calculated *RL* in Table 1 reveals desirable adsorption (*RL* < 1). According to Langmuir isotherm, the maximum adsorption capacities (q_{max}) for the MNPsH1, MNPsH2, and MNPsH3 were 28.92, 28.11 and 29.27 (mg/g), respectively. From the Freundlich isotherm, the value of (*1/n*) for all three samples was between 0 and 1, which was reported as a suitable factor. Fig. 15 illustrates the non-linear plots of Langmuir, Freundlich and Temkin [34].

In vitro release behavior of hydrogels

DS is an anti-inflammatory and analgesic drug with the site of action at the beginning of the rectum in the body. This drug was selected as a sample and model for controlled release. Releasing DS from MNP_SH was conducted in PBS (PH: 7.4) at 37 °C in vitro. The percentage of released drugs from MNP_SH was plotted as a function of time. As illustrated in Fig. 16, complete releasing of all DS from MNP_SH was 88, 91 and 93% in 120 min for MNP_SH1, MNP_SH2 and MNP_SH3, respectively. MNP_SH3 assigned the most significant time of releasing to itself. This occurred because of the rise in the extent of MNP_S of the lattice formed on the smaller network MNP_SH and the slower rate of DS. Moreover, in vitro release data were analyzed using kinetics equivalents (8, 9 and10) to confirm the release mechanism of DS from MNP_SH at PH: 7.4 at 37 °C [35].

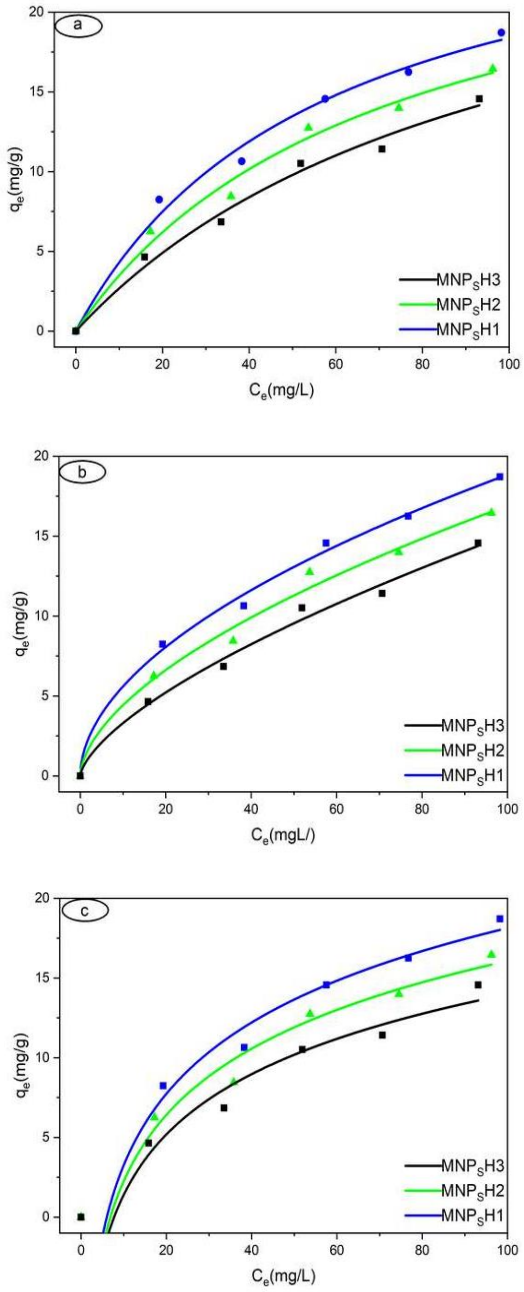

Fig. 15: Non-linear fitting plots of the Langmuir a) Freundlich, b) Temkin and c) Isotherm.

First-order kinetics:

$$\left[\frac{M_t}{M_e}\right] = 1 - \exp^{(kt)} \quad (8)$$

Second- order kinetics:

$$\left[\frac{t}{M_t}\right] = \left[\frac{1}{kM_e^2}\right] + \left[\frac{t}{M_e}\right] \quad (9)$$

Table 1: Isotherm parameters of adsorption of MNPsH1, MNPsH2 and MNPsH3.

Model	Factors	MNPsH1	MNPsH2	MNPsH3
Langmuir	b (L/mg)	0.017	0.014	0.010
	q_{max} (mg/g)	28.92	28.11	29.27
	RL	0.37	0.41	0.50
	R^2	0.99	0.99	0.99
Freundlich	K_f (L/g)	1.69	1.15	0.79
	1/n	0.52	0.58	0.65
	n	1.92	1.72	1.54
	R^2	0.98	0.97	0.98
Temkin	β (L /g)	0.16	0.14	0.13
	k_t	6.46	6.00	5.46
	R^2	0.97	0.97	0.96

Table 2: Kinetic parameters of DS release of MNPsH1, MNPsH2 and MNPsH3.

Model	Factors	MNP_SH1	MNP_SH2	MNP_SH3
First- order *kinetics*	R^2	0.97	0.91	0.79
	K_1	0.029	0.012	0.042
Second- order kinetics	R^2	0.98	0.92	0.87
	K_2	0.030	0.005	0.055
Ritger-Peppas	n	0.47	0.60	0.33
	k	1.21	1.46	1.10
	R^2	0.98	0.96	0.98

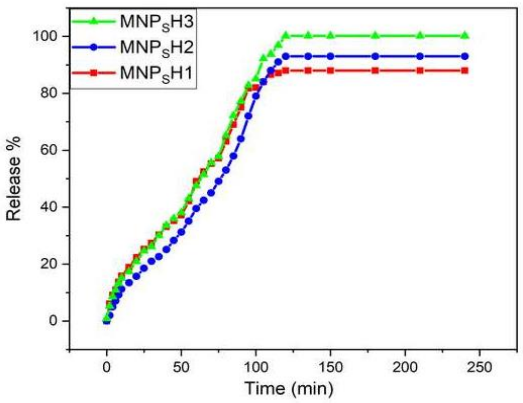

Fig. 16: Releasing of DS from MNPsH carrier as a function of time. Conditions: Concentration of DS, 100 mg/L; pH: 7.4 and temperature: 37 ℃.

Ritger-Peppas model:

$$\left[\frac{M_t}{M_e}\right] = kt^n \qquad (10)$$

Where *t* refers to the release time (min) of the MNP_SH; *Mt* and *Me* represent the amount of release at time *t* and equilibrium, respectively. *K* is a kinetic constant, and *n* is a characteristic diffusion exponent representing the release mechanism. If the values of n are below 0.45, in the range 0.45–0.89 and above 0.89, the diffusion mechanism can be Fickian, non-Fickian, case II transport, or super case II transport separately. The results of the kinetics study using the above equations are presented in Table 2. Based on the results, it can be concluded that the release behavior of the MNP_SH is consistent with the Ritger-Peppas model, and its diffusion type is the case of Ritger-Peppas as well as diffusion mechanism for MNP_SH1 and MNP_SH2 non-Fickian and MNP_SH3 Fickian [36].

CONCLUSIONS

In the present study, MNP_SH bead was successfully prepared. FT-IR, TEM, SEM, EDS, XRD, VSM, TGA, and DTG confirmed the presence of MNP_S and MNP_SH structures. The thermal stability of the MNP_SH was increased after the incorporation of MNP_S used as a cross-linker in the synthesis of MNP_SH. DS was loaded at MNP_SH with different amounts of cross-linker, and it

was released in the neutral buffer medium with a pH: of 7.4. The best performance was related to the MNP_SH with the highest cross-linking. The adsorption isotherm of DS was also examined by Langmuir, Freundlich, and Temkin models. The results indicated that the adsorption isotherm corresponds to the Langmuir equation. Kinetics of drug release with first- and second-order rates and the Ritger-Peppas model were mulled over. In addition, the DS drug at pH: 7.4 with Ritger-Peppas, MNP_SH1, MNP_SH2 Fickian, and MNP_SH3 non-Fickian was reported. The outcomes provided valuable information and insights on the use of MNP_SH for biomedical, color, and heavy metal absorption and catalysis applications.

Acknowledgments

The authors sincerely appreciate the instrumental supports of this work by Islamic Azad University- Karaj Branch

Received : Jun. 31, 2022 ; Accepted : Oct. 10, 2022

REFERENCES

[1] Barbucci R., et al., A Novel Strategy For Engineering Hydrogels with Ferromagnetic Nanoparticles as Crosslinkers of the Polymer Chains. Potential Applications as a Targeted Drug Delivery System, *Soft Matter*, **7(12)**: 5558–5565 (2011).

[2] Rezanejade Bardajee G., Asgari SH., Mirshokraie Se. Ah, Submicron Particles of Double Network Alginate/Polyacrylamide Hydrogels for Drug Delivery of 5-Fluorouracil, *Iran. J. Chem. Chem. Eng. (IJCCE)*, **40(5)**: 1386-1394 (2021).

[3] Bogdashkina D.V., Makhaeva E.E., Khokhlov A.R., Features of the Interaction of Alcian Blue with Gels Based on Copolymer of N-Vinylcaprolactam and Methacrylic Acid, *Polym. Sci. A*, **60(2)** (2018).

[4] Nishi K., Akizuki S., Toda T., Matsuyama T., Ida J., Development of Light-Shielding Hydrogel for Nitrifying Bacteria to Prevent Photoinhibition under Strong Light Irradiation, *Process Biochem.*, **94**: 359–364 (2020).

[5] Taghavi Fardood Sa., Ebadzadeh Be, Ramazani A., Green Synthesis and Characterization of Ni-Cu-Mg Ferrite Nanoparticles in the Presence of Tragacanth Gum and Study of Their Catalytic Activity in the Synthesis of Hexanitrohexaazaisowurtzitane. *Iran. J. Chem. Chem. Eng. (IJCCE)*, **38** (6): 21-29 (2019).

[6] Zhang Y. Ding Z. Liu Y. Zhang Y,. Jiang S., White-Light-Emitting Hydrogels with Self-Healing Properties and Adjustable Emission Colors, *J. Colloid Interface Sci.*, **582**: 825–833 (20201).

[7] Kurdtabar M., Koutenaee R.N.,Rezanejade Bardajee G., Synthesis and Characterization of a Novel pH-Responsive Nanocomposite Hydrogel Based on Chitosan for Targeted Drug Release, *J. Polym. Res.* **25(5)**: 1–11 (2018).

[8] Chou F.-Y., Shih C.-M., Tsai M.-C., Chiu W.-Y., Lue S. J., Functional Acrylic Acid as Stabilizer for Synthesis of Smart Hydrogel Particles Containing a Magnetic Fe_3O_4 Core, *Polymer (Guildf).*, **53(14)**: 2839–2846 (2012).

[9] Hu X., Wang Y., Zhang L., Xu M., Zhang J., Dong W., Design of a pH-Sensitive Magnetic Composite Hydrogel Based on Salecan Graft Copolymer and Fe_3O_4@ SiO_2 Nanoparticles as Drug Carrier, *Int. J. Biol. Macromol.* **107**: 1811–1820 (2018)

[10] Kumar S., Prasad M., Rao R.,Topical Delivery of Clobetasol Propionate Loaded Nanosponge Hydrogel for Effective Treatment of Psoriasis: Formulation, Physicochemical Characterization, Antipsoriatic Potential and Biochemical Estimation, *Mater. Sci. Eng. C*, **119**: 111605 (2021).

[11] Siglreitmeier M,. et al., Multifunctional layered Magnetic Composites, *Beilstein J. Nanotechnol.*, **6(1)**: 134–148 (2015).

[12] Mahfoudhi N., Boufi S., Poly (Acrylic Acid-co-Acrylamide)/Cellulose Nanofibrils Nanocomposite Hydrogels: Effects of CNFs content on the Hydrogel Properties, *Cellulose*, **23(6)**: 3691–3701 (2016).

[13] Chen J., et al., Recent Advances in Mechano-Responsive Hydrogels for Biomedical Applications, *ACS Appl. Polym. Mater.*, **2(3)**:1092–1107 (2020).

[14] Cheng S., et al. Highly Efficient Removal of Antibiotic from Biomedical Wastewater Using Fenton-Like Catalyst Magnetic Pullulan Hydrogels, *Carbohydr. Polym.*, **262**: 117951 (2021).

[15] El-saied H.A., El-Fawal E.M., Green Superabsorbent Nanocomposite Hydrogels for High-Efficiency Adsorption and Photo-Degradation/Reduction of Toxic Pollutants from Waste Water, *Polym. Test.*, **97**: 107134 (2021).

[16] Mortazavi-Derazkola S., Salavati-Niasari M., Khojasteh H., Amiri O., Ghoreishi S.M., Green Synthesis of Magnetic Fe_3O_4/SiO_2/HAp Nanocomposite for Atenolol Delivery and in Vivo Toxicity Study, *J. Clean. Prod*., **168**: 39–50 (2017).

[17] Li J., Mooney D.J., Designing Hydrogels for Controlled Drug Delivery, *Nat. Rev. Mater*., **1(12)**: 1–17 (2016).

[18] Griffete N., Fresnais J., Espinosa A., Wilhelm C., Bée A., Ménager C., Design of Magnetic Molecularly Imprinted Polymer Nanoparticles for Controlled Release of Doxorubicin under an Alternative Magnetic Field in Athermal Conditions, *Nanoscale*, **(45)**: 18891–18896(2015).

[19] Wang J., Zheng S., Shao Y., Liu J., Xu Z., Zhu D., Amino-Functionalized $Fe_3O_4@SiO_2$ Core–Shell Magnetic Nanomaterial as a Novel Adsorbent for Aqueous Heavy Metals Removal, *J. Colloid Interface Sci.*, **349(1)**: 293–299 (2010).

[20] Fekri M.H., Tousi F., Heydari R., Razavi Mehr M., Rashidipour M,. Synthesis of Magnetic Novel Hybrid Nanocomposite ($Fe_3O_4@SiO_2$/Activated Carbon(by a Green Method and Evaluation of Its Antibacterial Potential. *Iran. J. Chem. Chem. Eng. (IJCCE)*, **41(3)**: 767-776 (2022).

[21] Taghvai Nakhjiri M., Bagheri Marandi G., Kurdtabar M., Adsorption of Methylene Blue, Brilliant Green and Rhodamine B from Aqueous Solution Using Collagen-gp (AA-co-NVP)/$Fe_3O_4@SiO_2$ Nanocomposite Hydrogel, *J. Polym. Environ*. **27** (3): 581–599(2019).

[22] Zheng X., Wang C., Dai J., Shi W., Yan Y., Design of mesoporous silica hybrid materials as sorbents for the selective recovery of rare earth metals. *J. Mater. Chem. A.* (19): 10327–10335 (2015).

[23] Bagheri Marandi G., R. Mahdavinia G., Ghafary S., Collagen-g-poly (Sodium Acrylate-co-Acrylamide)Sodium Montmorillonite Superabsorbent Nanocomposites: Synthesis and Swelling Behavior, *J. Polym. Res.*, **18(6)**: 1487–1499 (2011).

[24] Khodabakhshi M.J., Panahi H.A., Konoz E., Feizbakhsh A., Kimiagar S., Synthesis of pH and Thermo-Sensitive Dendrimers Based on MoS_2 and Magnetic Nanoparticles for Cisplatin Drug Delivery System by the Near-Infrared Laser, *Polym. Adv. Technol*., **32(4)**: 1626–1635 (2021).

[25] Li X., Zhang Z., Chen H., Development and Evaluation of Fast Forming Nano-Composite Hydrogel for Ocular Delivery of Diclofenac, *Int. J. Pharm*.**, 448(1)**: 96–100 (2013).

[26] Xu J., et al. Synthesis and Characterization of Magnetic Nanoparticles and its Application in Lipase Immobilization, *Bull. Korean Chem. Soc*., **34(8)**: 2408–2412 (2013).

[27] Yang Li., Tian J., Meng J., Zhao R., Li C., Ma J., Jin T., Modification and Characterization of Fe_3O_4 Nanoparticles for Use in Adsorption of AlKaloids, *J. Molecules.*, **23**: 562 (2018).

[28] Facchi De.P., Cazetta A.L., Canesin E.A., Almeida V.C., Bonafe E.G., Kipper M.J., Martins F., New Magnetic Chitosan/Alginate/ $Fe_3O_4@SiO_2$ Hydrogel Composites Applied for Removal of Pb(II) Ions Aqueous Systems, *Chemical Engineering Journal*, **337**: 595–608 (2018).

[29] Karimi., Bagherian F., Karimi M., Cu-phthalocyanine Coated Hybrid Magnetic Nanoparticles: Preparation and Application in the Synthesis of Mono- and Bis pyrano[2,3-d]pyrimidinones and Mono- and Bis-2-amino-4H-pyrans, *Iran. J. Chem. Chem. Eng. (IJCCE)*, **39(2)**: 21-31 (2020).

[30] Kurdtabar M., Rezanejade Bardajee G., Drug Release and Swelling Behavior of Magnetic Iron Oxide Nanocomposite Hydrogels Based on Poly (Acrylic Acid) Grafted onto Sodium Alginate, *Polym. Bull.*, **77(6)**: 3001–3015(2020).

[31] Zahra Q., Minhas M S., Khan S., Wu P., Suhail M., Iqbal R., Bashir M., Fabrication of Polyethylene Glycol Hydrogels with Enhanced Swelling; Loading Capacity and Release Kinetics, *Polym. Bull.*, **79(5)**: 5389-5415 (2022).

[32] Bardajee G., Asgari Sh., Mirshokraie A., Submicron Particles of Double Network Alginate/ Polyacrylamide Hydrogels for Drug Delivery of 5-Fluorouracil. *Iran. J. Chem. Chem. Eng. (IJCCE)*, **40(5)**: 1386-1394 (2021).

[33] Dangia D., Mattoo M., Kumara V., Sharma P., Synthesis and Characterization of Galactomannan Polymer Hydrogel and Sustained Drug Delivery, *Carbohydrate Polymer Technologies and Applications*, **4:** 100230 (2022).

[34] Zarei Sh., R. Rezanejade Bardajee G., Sadeghi M., Montmorillonite Nanocomposite Hydrogel Based on Poly (acryilcacid-co-acrylamide): Polymer Carrier for Controlled Release Systems, *Iran. J. Chem. Chem. Eng. (IJCCE)*, **38(5)**: 9986-1021 (2019).

[35] Rashidi Z., Bagheri Marandi G., Taghvai Nakhjiri M., Carboxymethyl Cellulose-Based Nanocomposite Hydrogel Grafted with Vinylic Comonomers: Synthesis, Swelling Behavior and Drug Delivery Investigation, *Journal of Macromolecular Science, Part A.*, **59(6)**: 421-432 (2022).

[36] Pourjalili N., Bagheri Marandi G., Kurdtabar M., Rezanejade Bardajee G., Synthesis and Characterization of Double Network Hydrogel Based on Gellan-Gum for Drug Delivery, *Journal of Macromolecular Science, Part A.*, **59(8)**: 537-549 (2022).